geosciences

MDPI

Article

Geomorphological and Morphometric Analyses of the Catanzaro Trough (Central Calabrian Arc, Southern Italy): Seismotectonic Implications

Claudia Pirrotta [1], Nicolò Parrino [2], Fabrizio Pepe [2], Carlo Tansi [3] and Carmelo Monaco [1,4,5,*]

[1] Dipartimento di Scienze Biologiche Geologiche e Ambientali, Università di Catania, 95129 Catania, Italy
[2] Dipartimento di Scienze della Terra e del Mare, Università di Palermo, 90123 Palermo, Italy
[3] Sede di Cosenza, CNR-IRPI, 87036 Rende, Italy
[4] CRUST—Interuniversity Center for 3D Seismotectonics with Territorial Applications, 66100 Chieti, Italy
[5] Istituto Nazionale di Geofisica e Vulcanologia, Osservatorio Etneo—Sezione di Catania, 95125 Catania, Italy
* Correspondence: cmonaco@unict.it; Tel.: +39-095-7195731

Abstract: In this work, we investigated the landscape response to the recent activity of the faults affecting the Catanzaro Trough, a seismically active structural basin that developed transversally to the Calabrian Arc (Southern Italy) during the Neogene–Quaternary. We carried out a geomorphological and morphometric study of the drainage networks and basins intercepted by the Quaternary faults that were previously mapped through remote and field analyses. The study confirms the occurrence north of the Catanzaro Trough of a WNW–ESE-oriented left-lateral strike-slip fault system (here named the South Sila Piccola Fault System), which accommodates the differential SE-ward migration of the upper crustal sectors of the Calabrian Arc, and of a south-dipping WNW–ESE-oriented oblique fault system (the Lamezia-Catanzaro Fault System), characterized by a predominant normal component of movement. The latter delimits the Catanzaro Trough and accommodates the transition from a strike-slip regime to an extensional regime in the south. Inside the Catanzaro Trough, we detected for the first time a NNE–SSW-trending, WNW-dipping fault system (here named the Caraffa Fault System). This system contributes to accommodate the extension that occurs orthogonally to the southern sector of the Calabrian Arc. The geomorphological and morphometric analysis revealed the recent activity of these fault systems. In particular, the activity of the Caraffa Fault System is evidenced by the differential uplift and tilting of discrete areas inside the basin. Given its location, geometry, and kinematics, the Caraffa Fault System could be responsible for the occurrence of large historical earthquakes.

Keywords: Calabrian Arc; active tectonics; geomorphology; morphotectonics; fluvial morphometry

Citation: Pirrotta, C.; Parrino, N.; Pepe, F.; Tansi, C.; Monaco, C. Geomorphological and Morphometric Analyses of the Catanzaro Trough (Central Calabrian Arc, Southern Italy): Seismotectonic Implications. *Geosciences* **2022**, *12*, 324. https://doi.org/10.3390/geosciences12090324

Academic Editors: M. Scott Harris, Niki Evelpidou, Charalampos Fassoulas and Jesus Martinez-Frias

Received: 19 July 2022
Accepted: 26 August 2022
Published: 29 August 2022

1. Introduction

Starting from the Pliocene, extensional and strike-slip tectonics deformed the pre-existing contractional framework of the Calabrian Arc (southern Italy, Figure 1A), resulting in the formation of basins oriented longitudinally and transversely to the orogen [1,2]. The Catanzaro Trough is a transversal basin located in the central Calabrian Arc, between two longitudinal basins: the Crati Basin to the north, adjacent to the Sila Massif, and the Mesima Basin to the south, adjacent to the Serre Mountains [3–6].

Despite the numerous geological studies carried out in this sector of the Calabrian Arc ([3–10], among others), the active tectonics of the area and the landscape response to Quaternary tectonics are not yet defined. Particularly, the role and recent activity of the WNW–ESE fault systems bordering the Catanzaro Trough to the north and south [6,8,11] and the extensional processes in it [9,12,13] are still poorly defined or matters of debate.

During historical times, several destructive earthquakes, with Mw up to 7.5 and maximum intensity XI, occurred in the Catanzaro Trough (Figure 1B), such as the 1626 event

(Io = IX and Mw = 6.07 [14]) and the 28 March 1783 event (Io = XI and Mw = 7.03 [14]), the latter being the last of a seismic sequence that destroyed the southern Calabria since 5 February 1783. Notwithstanding the several seismogenic sources parametrized in the central Calabrian Arc [15], only the NNE–SSW exploratory source modelled by Akinci et al. [13] (ITES002; see Figure 1B) might be suitable for these events. However, this is a working hypothesis based on geodynamic considerations not constrained by structural field evidence or by morphometric signature.

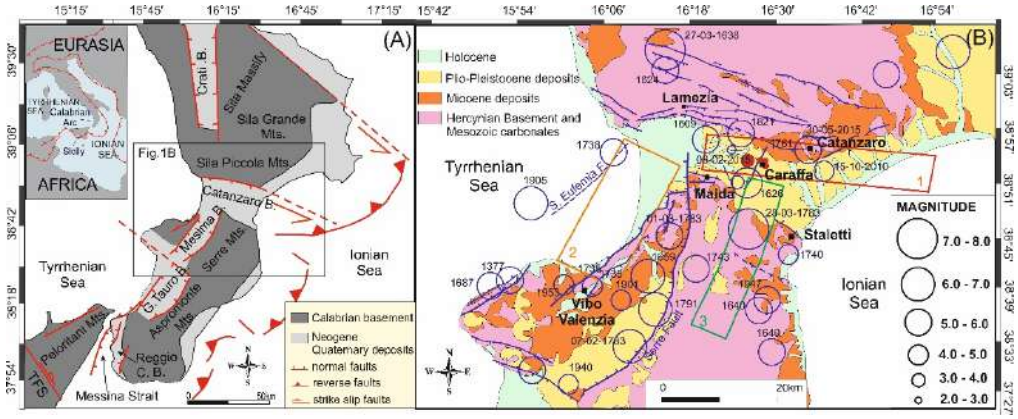

Figure 1. (**A**) Simplified map showing the main structural elements of the Calabrian Arc (from 9 modified). TFS, Tindari Fault System. Inset shows the central Mediterranean orogen in the context of the Eurasia–Africa convergence. (**B**) Geological map of the Catanzaro Trough and the surrounding area showing Quaternary faults from the literature (see Figure 1A for location). Circles are the historical and instrumental epicentres of earthquakes with a magnitude higher than 4.8 (CPTI,14); red balls represent the seismic sequence of October 2019; rectangles are modelled seismogenic sources: 1, ITCS068; 2, ITCS110 (from the database of the DISS Working Group [15]); 3, ITES002 (from Akingi et al. [13]).

Morphometric analysis has proved to be particularly efficient in detecting the tectonic force on the landscape evolution, highlighting the activity of blind or elusive faults where intense erosion rapidly erases their morphological signature [16–20]. Numerous authors successfully applied morphometric approaches based on the drainage network hierarchy evaluation, the computation of catchment and drainage pattern metrics, the relief distribution, and river longitudinal profile analyses to highlight recent differential vertical movements [20–27], even in the northern and southern sectors of the Calabrian Arc [28–30].

In this paper, we analyse the recent fault activity in the Catanzaro Trough, trying to define the potential seismogenic sources through (i) the morphostructural study of the fault systems, (ii) the qualitative geomorphological and quantitative morphometric investigations of the drainage network and related basins, (iii) the computation of hierarchical parameters and geomorphic indices (e.g., hypsometric integrals and normalized stream-length gradient), and (iv) the critical review and new interpretation of the most updated geodetic and seismological dataset published.

2. Geological Setting

2.1. Geodynamic Framework

The geodynamic evolution of the Calabrian Arc and its adjacent offshore sectors (Figure 1) is controlled by the north-westward subduction of the oceanic Ionian lithosphere, which, being confined between two continental sectors (the Apulian block, to the north and the Pelagian block, to the south), has led the bowing of this sector of the orogen and the development of a complex Neogene–Quaternary backarc/forearc/trench system [31–39]. Currently, the subduction of the Ionian lithosphere occurs only in a segment of the arc between the Tindari Fault System to the south (TFS in Figure 1A) and the Catanzaro Trough to the north [34,40–44]. North of the Catanzaro Trough, left-lateral strike-slip fault systems

accommodate in the upper plate the gradual transition from subduction in the Calabrian Arc to collision in the Southern Apennines [6,7].

Quaternary post-orogenic extension perpendicular to the arc and coeval regional uplift, likely due to asthenosphere wedging or incipient slab detachment [40,45–48], caused the development of several systems of normal faults [1–4,8,9,35,38]. Such a tectonic phase triggered the formation of basins oriented longitudinally to the orogenic trend, e.g., Crati, Mesima, Gioia Tauro, and Messina Strait, interrupted by transversal basins, e.g., Sibari, Reggio Calabria, and the Catanzaro Trough [1] (Figure 1A). The Catanzaro Trough is a WNW–ESE-trending Late Neogene to Quaternary basin that separates the northern and southern parts of the Calabrian Arc [5–7]. Recently, the Catanzaro Trough has been interpreted as a semigraben structured by the polyphase activity of the Lamezia–Catanzaro Fault System that delimits the basin to the north, representing the upper plate expression of a deep-tear fault [9,34] related to the transition from the subduction to the collisional domain.

2.2. Geological, Geomorphological, and Structural Features of the Catanzaro Trough

The Neogene to Quaternary terrigenous sequences of the Catanzaro Trough unconformably lie on the structural units of the Calabrian Arc (Figure 1B), made up of metamorphic and magmatic rocks of the Hercynian basement and by Mesozoic platform carbonates [12,49,50]. The top of the sedimentary succession is constituted by four orders of Middle–Upper Pleistocene marine terraces, made of siliciclastic sands and sandstones [8,12] (Figure 2B). Due to regional uplift, combined with the activity of Quaternary faults [45], the terraced deposits are distributed at different elevations. An extensive system of coalescent Pleistocene alluvial fans, lateral to the III order terrace, occurs in the northwestern sector of the Catanzaro Trough (Figure 2B).

The Lamezia–Catanzaro Fault System borders the Catanzaro Trough to the north and separates the Calabrian Arc units from the Neogene–Quaternary sequences (Figure 2). It is roughly 40 km long and constituted by minor 10–15 km long, WNW–ESE and WSW–ENE-striking, oblique-slip faults locally arranged in a left-stepping en echelon pattern [8,12]. According to Pirrotta et al. [9], it is characterized by a left-lateral component of motion along the WNW–ESE-striking fault planes and by a prevalent normal (slightly right-lateral) motion along the WSW–ENE-oriented planes. Morphological evidence highlights a prevalence of normal faulting during the late Pleistocene [9]. Inside the Catanzaro Trough, N–S to NNE–SSW normal faults, with a minor right-lateral component of motion and limited displacement at the surface, offset Tortonian to Pliocene and lower Pleistocene deposits [12]. Minor north-dipping normal faults, about 9–10 km long and WNW–ESE-oriented, characterize the southern margin of the basin, the most developed of which are the Maida Fault and the Staletti Fault (Figure 2A). North of the Catanzaro Trough, a strike-slip fault system affects the southern sector of the Sila Piccola Massif. It is part of a Middle Miocene–Middle Pleistocene left-lateral strike-slip shear zone (Sellia-Decollatura fault zone of Van Dick et al. [7] and Amantea-Gimigliano fault of Tansi et al. [6]).

In the northern and central sectors of the Catanzaro Trough, active tectonics are evidenced by clusters of earthquakes and by geodetic data indicating slow left-lateral motion along the Lamezia–Catanzaro Fault System and extension inside the basin [9]. In particular, these data support the occurrence of a NNE–SSW-oriented extensional fault system belonging to the alignment of the Serre Fault (Figure 2A), a major structure that accommodates to the south the extension orthogonal to the Calabrian Arc.

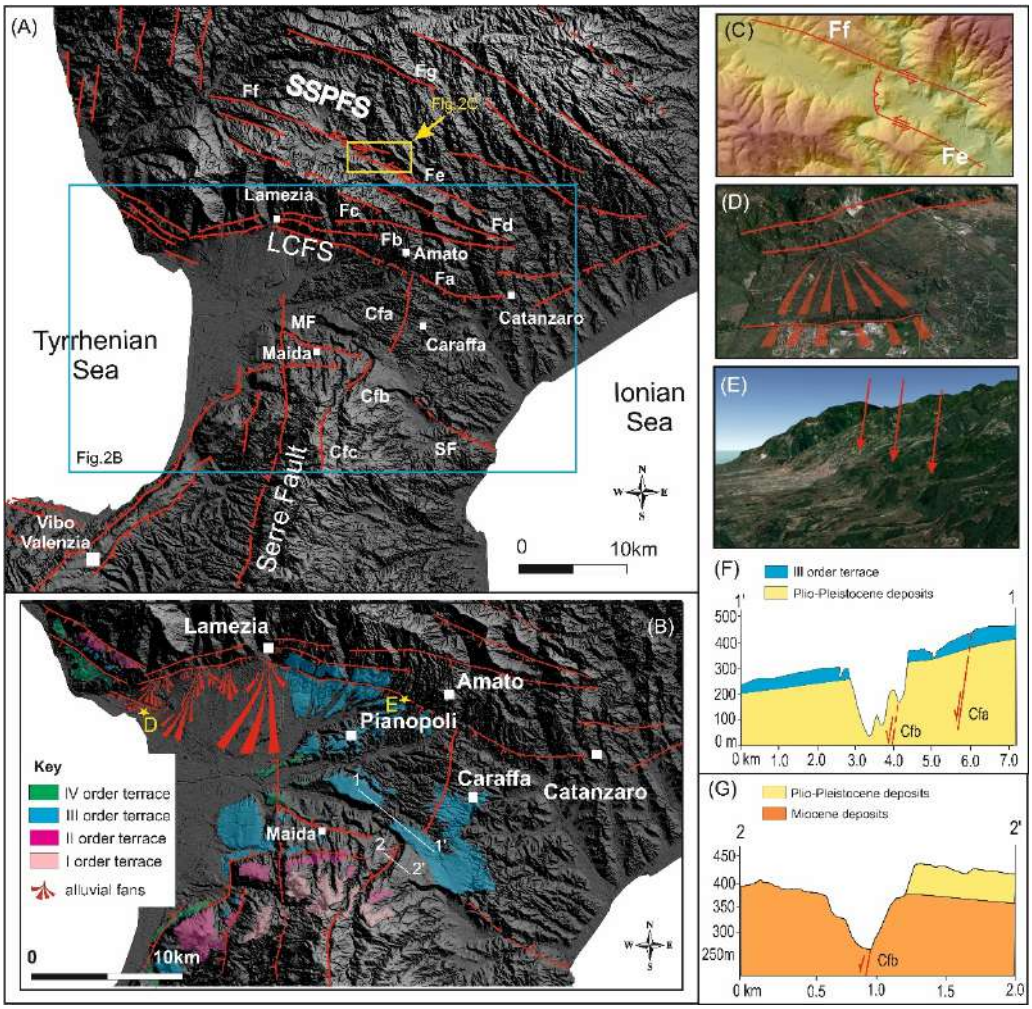

Figure 2. (**A**) DTM hillshade and fault pattern of the Catanzaro Trough area. SSPFS, South Sila Piccola Fault System; LCFS, Lamezia–Catanzaro Fault System; MF, Maida, Fault; SF, Stalettì Fault. Cfa, Cfb, and Cfc are the segments of the Caraffa Fault System. (**B**) DTM hillshade (see Figure 2A for location) showing alluvial fans, faults (dashed where inferred), and colour-coded upper Middle–Upper Pleistocene terraces (modified from Brutto et al. [8] and Gullà et al. [12]); stars indicate the location of Figure 2D,E. (**C**) Push-up ridge between Fe and Ff at the Serrastretta locality (see Figure 2A for location). (**D**) Displaced alluvial fan (see Figure 2B for location). (**E**) Trapezoidal facets created by Fa north of Pianopoli (see Figure 2B for location). (**F**) Schematic geological profile showing the III order terrace warped and tilted by the Cfa and Cfb faults. (**G**) Schematic geological profile showing the Cfb fault scarp and the asymmetric valley.

3. Methods and Analysis

Our research involved the following methods: (1) joint interpretation of aerial photos and Digital Terrain Models (DTM) to detect morphological evidence of active faults, (2) geomorphological and morphometric investigations of the drainage networks and hydrographic basins to analyse the landscape response to the tectonic forcing of active faults, and (3) a combined review of the seismicity catalogues and the GNSS velocity field to validate the recent activity of the faults.

In order to review the active faults reported in the literature and to check the accuracy of their position, we analysed the 5 m geometrical resolution LIDAR-derived DTM (Digital Terrain Model) provided by the Calabria Region (http://geoportale.regione.calabria.it/, accessed on 1 January 2021, projected in WGS 1984 UTM Zone 33N) and the aerial stereopairs provided by the Italian Military Geographical Institute (1:33.000 scale, https://www.igmi.org/it/

descrizione-prodotti/aerial-photography/black-and-white-or-colour-aerial-photographs, accessed on 1 January 2021).

The qualitative geomorphological analysis was focused on the geomorphological markers indicating landscape response to tectonic forcing, such as offset, tilted, and warped terraces; morphological scarps; and fluvial deflections and piracies near the Quaternary outcropping or elusive faults [22,27,28,51,52]. We analysed these markers both in map view and on longitudinal profiles. In detail, we extracted two profiles along alignments of drainage divide tracts: one orthogonal to the Catanzaro Trough (A-A′ in Figures 3A and 4A) and the other longitudinal to the trough (B-B′ in Figures 3A and 4B). The main advantage of the investigation of the drainage divide is that along its track, the erosive processes influence the landscape less, and the effects of the tectonic perturbation are more evident [29]. In addition, we reconstructed a 6 km wide, 35 km long, W–E-trending swath profile extending from the Tyrrhenian towards the Ionian coast (C-C′ in Figures 3A and 4C). Finally, we extracted the longitudinal profile of minor river channels for more detailed evaluations (R1–R5 in Figures 3C and 5A–E). These profiles were smoothed using a first-order polynomial LOESS filter with the nearest neighbour's bandwidth method and a 0.1 sampling proportion.

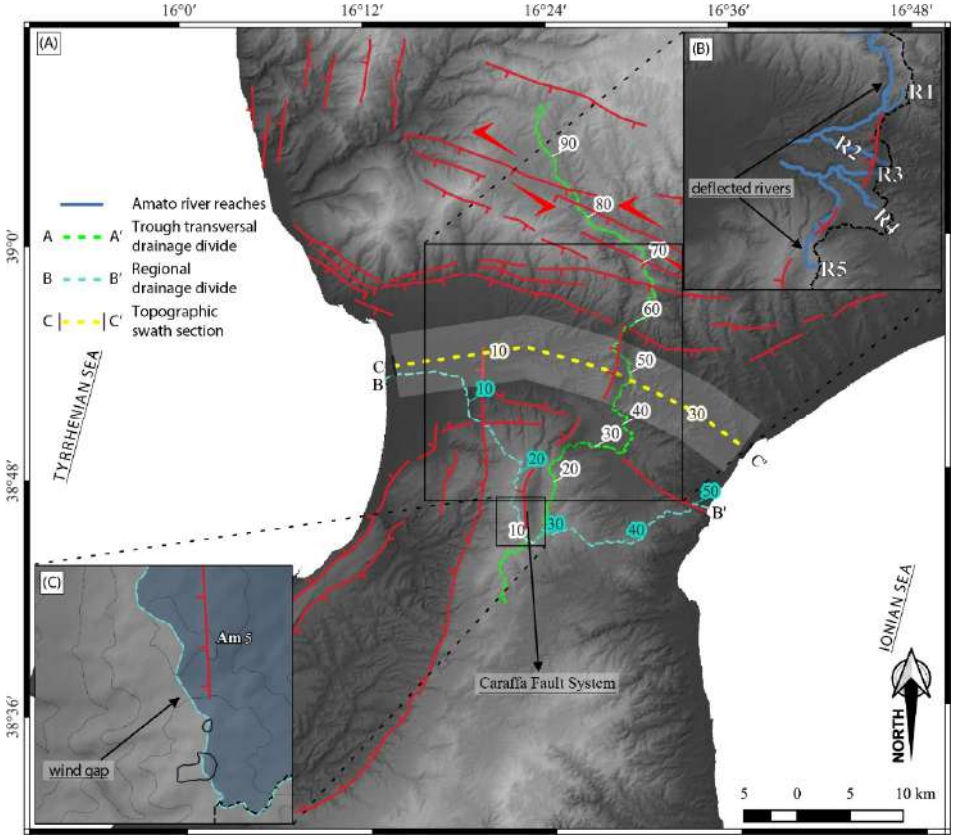

Figure 3. (**A**) Hillshade visualization of the Digital Elevation Model (DEM) of Central Calabria. The green dashed line A-A′ indicates the trace of the drainage divide transversal to the Catanzaro Trough (the profile is plotted in Figure 4A); the cyan dashed line B-B′ is the trace of the regional drainage divide crossing out the Catanzaro Trough (the profile is plotted in Figure 4B). The yellow dashed line C-C′ and the semi-transparent white polygon represent the baseline and area sampled by the topographic swath profile plotted in Figure 4C. Numbers indicate the along-trace distance expressed in km. (**B**) Map view of the main reaches of the Amato River crossed out or deflected by the Caraffa Fault System; the profiles of the reaches R1–R5 are plotted in Figure 5A–E. (**C**) Map view of a significant wind gap along trace B-B′ (see also Figure 4B).

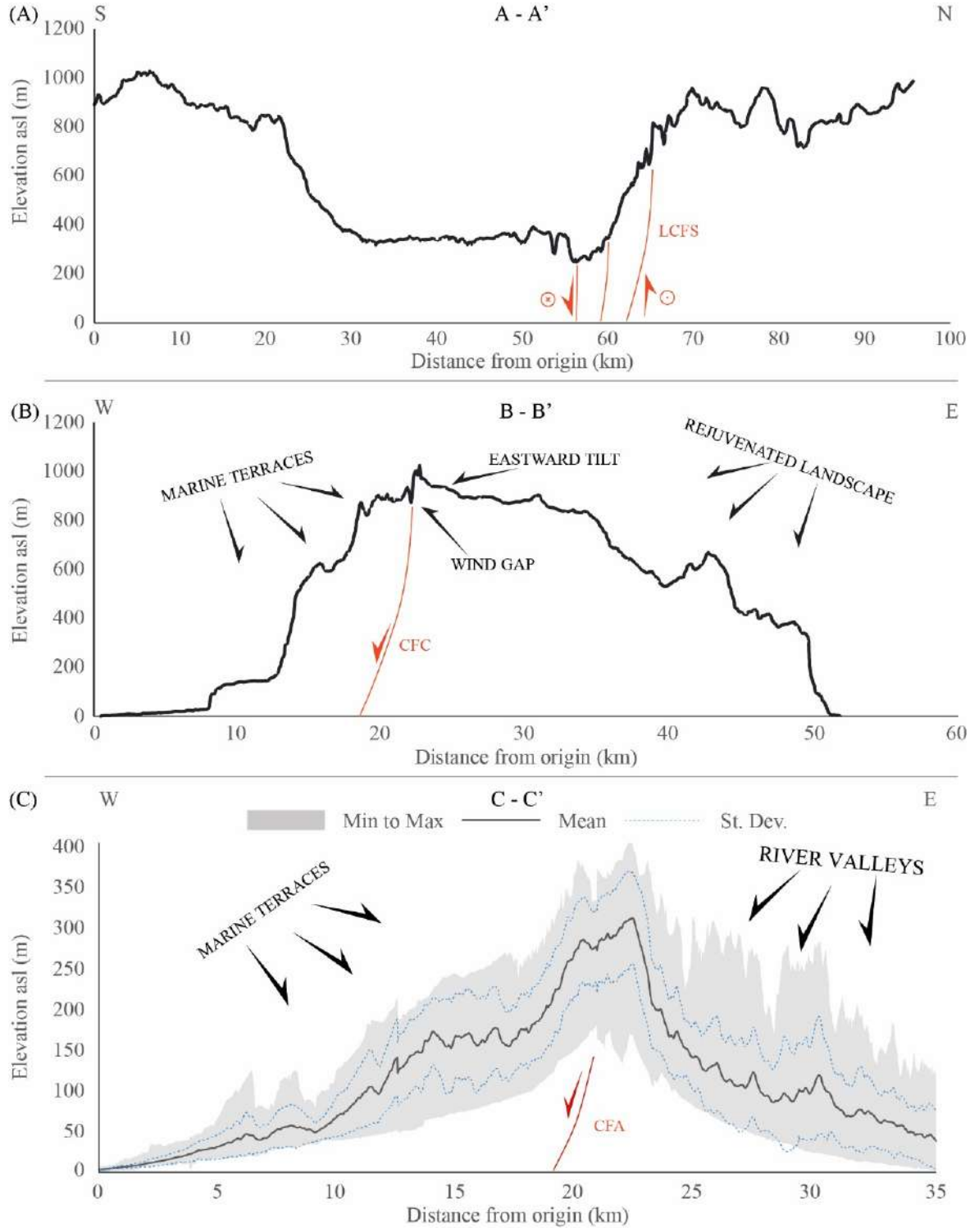

Figure 4. (**A**) Topographic profile along the A-A′ trace. (**B**) Topographic profile along the B-B′ trace. The trace of both profiles is reported in the map of Figure 3A. (**C**) Swath profile across the Catanzaro Trough (see Figure 3A for the trace).

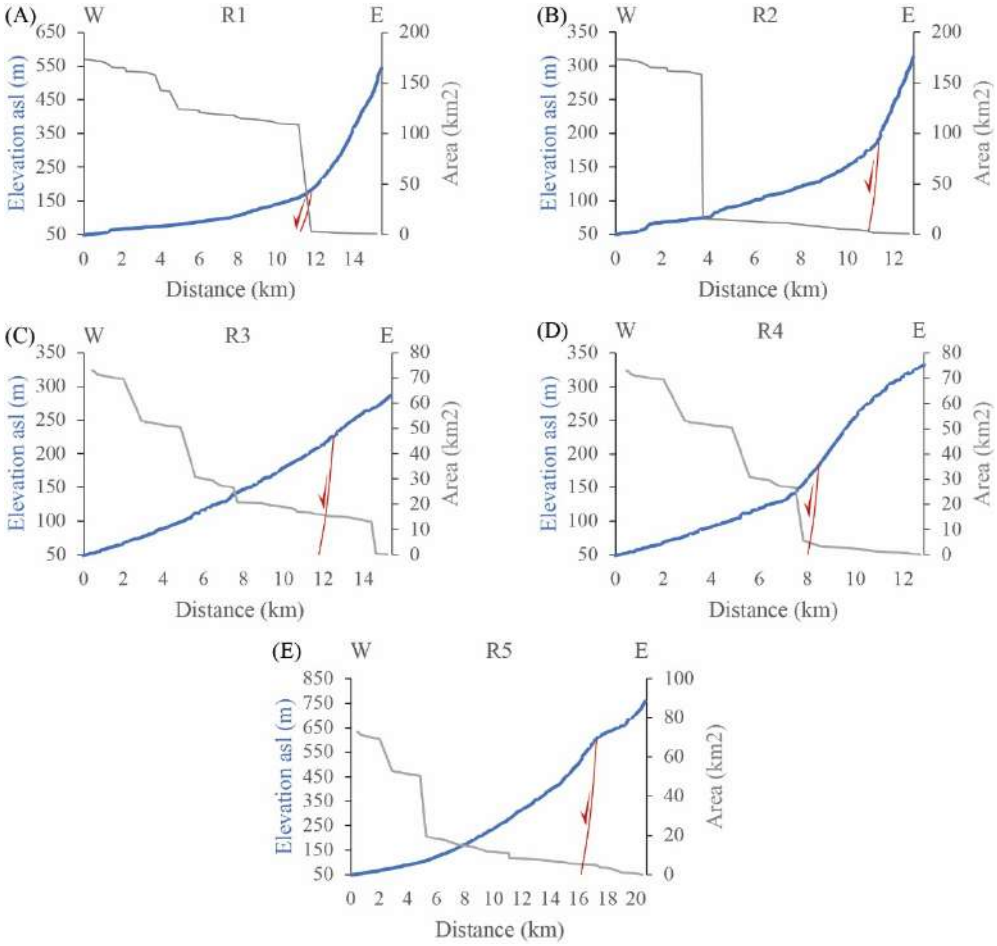

Figure 5. (**A**–**E**) Longitudinal profiles (blue lines) of the R1–R5 reaches of the Amato River, respectively (see Figure 3B for the traces), against catchment areas (grey lines).

The quantitative morphometric analysis focuses on 17 sub-basins extracted from six main basins flowing into the Catanzaro Trough, selecting as outlets each intersection between rivers stems and the 50 m a.s.l. contour line (Figure 6A,B). The digital network of the drainage was obtained using the D8 approach [53] and a minimum mappable outflow of 20,000 square meters. For the extracted sub-basins, we computed some landscape parameters, such as slope degree and local relief, by using a square moving window of 500 m per side (Figure 6C,D) and some geomorphic indexes such as the normalized steepness index Ksn and the transverse topographic basin asymmetry index T-factor (Figure 6B,E; see Table 1 for the description). To compare the literature data, we calculated the sub-basin averaged Ksn values using a reference concavity of 0.45. The T-factor was extracted following the Cox's [16] methodology through an in-house developed geospatial model, sampling the basin midlines every 100 m [52].

We applied a further quantitative investigation to three sub-basins: the Am4 and the C2 in the northern sector and the A1 in the southern sector of the basin (Figures 6F, 7 and 8). Am4 and C2 were extracted for this analysis, selecting the slope break of the South Sila Piccola massif as outlets. We calculated the hierarchical drainage parameters (Strahler order; bifurcation ratio; direct bifurcation ratio; bifurcation index, R; anomaly parameter, An) and geomorphic indexes (asymmetry factor, AF; basin elongation ratio, Re; sinuosity index, S; hypsometric integral curve; see Table 1 for the description) and extracted the longitudinal profile of the main river trunks. Lithology, local climate, and human causes, which can influence the geomorphic indexes' evaluation, were also considered during the morphometric analysis.

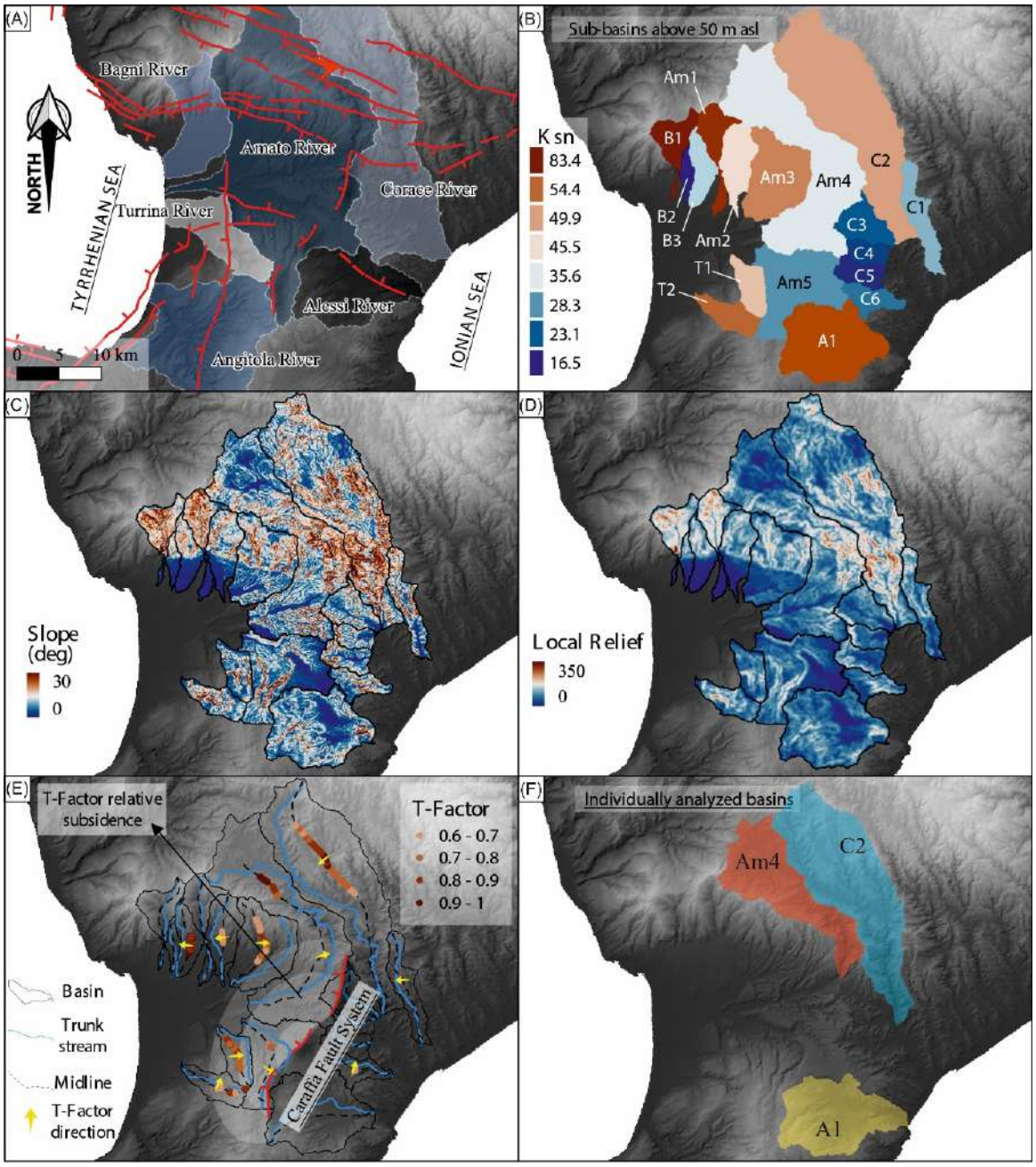

Figure 6. (**A**) Hillshade visualization of the Digital Elevation Model (DEM) of the analysed river basins considered for the analysis. (**B**) B1-3, sub-basins of the Bagni River; Am1-5, sub-basins of the Amato River; C1-6, sub-basins of the Corace River; T1-2, sub-basins of the Turrina River; A1, sub-basin of the Alessi River. Ksn values of each sub-basin. (**C**) Slope analysis; values are in degrees. (**D**) Local relief trend. (**E**) T-factor represented by coloured bars; yellow arrows indicate the direction of migration of the main river trunk. (**F**) Sub-basins further analysed through the morphometric approach.

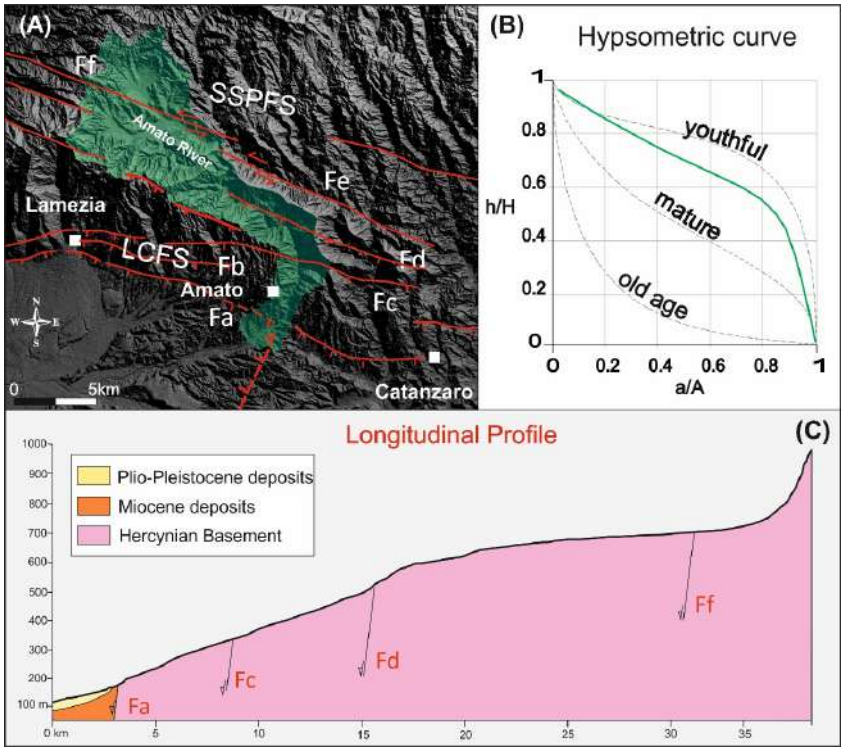

Figure 7. (**A**) DTM hillshade showing the Am4 sub-basin and the faults crossing the area. (**B**) Hypsometric curve of the Am4 sub-basin. (**C**) Longitudinal profile of the main river trunk of the Am4 sub-basin and faults.

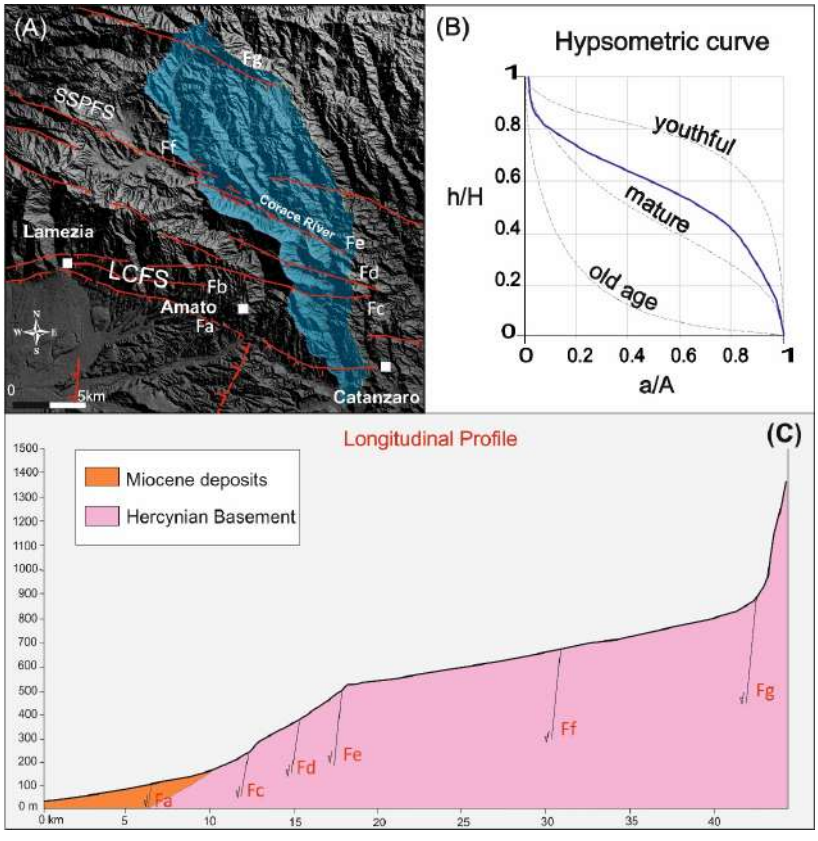

Figure 8. (**A**) DTM hillshade showing the C2 sub-basin and faults crossing the area. (**B**) Hypsometric curve of the C2 sub-basin. (**C**) Longitudinal profile of the C2 sub-basin and faults.

Fault activity and relative motions were validated (see Section 5) by published geodetic data [9] and instrumental seismicity (http://terremoti.ingv.it/, accessed on 15 July 2022, see also [54]).

Table 1. Hierarchical parameters and geomorphic indexes.

Hierarchical Parameters	Description	References
Strahler order	It indicates the phase of maturity of the hydrographic network. The hierarchical number is the highest order of the stream network.	[55,56]
Bifurcation ratio	It describes the degree of branching of the hydrographic network and highlights possible hierarchical anomalies. **Rb (u — u + 1) = Nu/Nu + 1** **Nu** is the number of fluvial segments of a given order; **Nu + 1** is the number of fluvial segments of the immediately higher order.	[55–57]
Direct bifurcation ratio	It describes the degree of branching of the hydrographic network and highlights possible hierarchical anomalies. **Rbd = Ndu/Nu + 1** **Ndu** represents the number of fluvial segments of a given order that flow into higher-order segments; **Nu + 1** is the number of segments of the next higher order.	
Bifurcation index (R)	It describes the degree of branching of the hydrographic network and highlights possible hierarchical anomalies. **R = Rb — Rdb** **Rb** encompasses all the segments of a given order, including the anomalous drainage, while **Rbd** considers only the non-anomalous segments. For a well-organized basin, **(Rb ≈ Rbd) R** must approach zero; on the contrary, high **R** values indicate that the fluvial network does not have an excellent hierarchical organization.	
Anomaly parameter	It indicates the fluvial anomalies. **An** i.e., a river segment of a given order *u* flowing into a segment of order *u* + 2. It is calculated for each *u* order.	[57]
Geomorphic Indexes	**Description**	**Reference**
Asymmetry factor	It allows the evaluation of the asymmetry of the basin. **AF = 100 (Ar/At)** where **Ar** is the basin area on the hydrographic right to the main river trunk segment; **At** is the area of the entire drainage basin. **AF** value greater than 50 indicates shifting towards the hydrographic left, whereas a value lower than 50 indicates rightward shifting.	[16,18,28,58]
Transverse topographic symmetry factor	It allows the evaluation of the asymmetry of the basin. **T = Da/Dd** where **Da** is the distance from the main river trunk to the basin midline; **Dd** is the distance from the basin watershed to the basin midline. Low **T** values indicate stability (**Da** approaches zero); on the contrary, **T** values approaching one indicate basin asymmetry and, thus, tilting.	[16]
Basin elongation ratio (Re)	It describes the planimetric shape of the basin and its phase of maturity and stability: a mature basin draining on a stable area has a shape similar to a circle, whereas a basin draining on an area characterized by a rapid uplift shows an elongated narrow shape. **Re = (2√A:√II)/Lb** where **A** is the basin area; **Lb** is the length of the basin parallel to the main drainage line.	[28,59]

Table 1. *Cont.*

Geomorphic Indexes	Description	Reference
Sinuosity index	It indicates the response of a fluvial channel to slope steepening with a meandering sinuosity increase. **S = L/Sl_Dist** **Sl_Dist** is the straight-line distance from the catchment start point to the endpoint, and **L** is the total length of the line segments. The sinuosity of a straight line is 1. If the line is closed (start point equals endpoint), the sinuosity is 0. As the line becomes curvier, the sinuosity increases.	[60] and references therein
Hypsometric integral	It quantifies the areal distribution of the relief elevation in the basin, describing the stage of the drainage basin or part of it, if youthful, mature, or old. Hypsometric integral is measured for an interval of elevation. The relative area (**a/A** ratio, with **A** total area and the basin area above a given elevation **h**, and the relative elevation (**h/H** ratio, with **H** maximum basin elevation and **h** topographic elevation), are represented in the Cartesian graph as a curve.	[56]
Normalized steepness index (K_{sn})	It represents a measure of the river channel slope nor-malized to the drainage area directly proportional to the uplift rates. $\mathbf{k_{sn}} = \frac{\mathbf{S}}{\mathbf{A}^{-\theta_{ref}}}$ **S** represents the slope, **A** the drainage area, and θ_{ref} the normalized channel concavity, set equal to 0.45, following the Kirby and Whipple (2012) approach. The normalized steepness index (**Ksn**) allows the comparison of stream profiles characterized by wildly varying drainage areas. Higher values indicate higher uplift rate values.	[20,61,62]

4. Geomorphological and Morphometric Evidence of Fault Activity

4.1. Structural Pattern

We analysed the following tectonic structures: (1) the WNW–ESE to ESE–WNW-trending, south-dipping Lamezia–Catanzaro fault system (LCFS: Fa, Fb, and Fc in Figure 2A), and the WNW–ESE-striking South Sila Piccola Fault System (SSPFS: Fd, Fe, Ff, and Fg in Figure 2A), both running to the north of the Catanzaro Trough; (2) the WNW–ESE-trending, north-dipping Maida Fault (MF in Figure 2A) and the Staletti Fault (SF in Figure 2A), both bordering the basin to the south; and (3) a newly detected NNE–SSW-trending, WNW-dipping fault system in the central sector of the basin, here named the Caraffa Fault System (Figure 2A). This system extends southwards with a segmented pattern (Cfa, Cfb and Cfc in Figure 2A) and a total length of about 17 km. The southernmost segment shows a N–S direction, parallel to the major Serre Fault (Figure 2A,B).

4.2. The South Sila Piccola and Lamezia–Catanzaro Fault Systems

The SSPFS shows evidence of recent left-lateral strike-slip activity at the Serrastretta locality where, during the Middle–Late Pleistocene, two over-stepping en echelon fault segments (Fe and Ff in Figure 2C) gave rise to a NNE–SSW-trending restraining sector (i.e., push-up structure), obstructing the drainage network and causing the formation of the Decollatura paleolake, characterized by Middle–Late Pleistocene lacustrine deposits [63].

In the northwestern sector of the study area, the LCFS is characterized by a set of fault steps that offset both upper Pleistocene marine terraces and alluvial fans (Figure 2B,D). These features, together with triangular and trapezoidal facets along the escarpment of Fa (Figure 2B,E), suggest the recent normal activity of the WNW–ESE-trending segment of the LCFS. The A-A' topographic profile (Figure 4A) shows the landscape imprint of the LCFS, characterized by morphological scarps and rejuvenation of the slope between the fault segments.

The activity of the SSPFS and the LCFS is evidenced by the morphometric analysis of the sub-basins flowing in the northern sector of the trough (i.e., B1-3, Am 1-4, and C1) (Figure 6A,F) that show the most significative multiple river flow deflections in the drainage network of the Catanzaro Trough (roughly 180° in the North Amato sub-basin, Figure 7A).

These sub-basins are characterized by medium to high values of Ksn (Figure 6B) and by increases in the values of slope and local relief at the footwall of the LCFS and, moderately, of the SSPFS (Figure 6C,D).

Regarding the analysis of the Am4 and C2 sub-basins, the values of the AF index (Table 2) and T-factor (Figure 6E) highlight a strong asymmetry and an anomalous shifting and convergence between the two main river trunks in the sector where the LCFS and the SSPFS intercept their drainage. These data indicate differential movements and tilting of discrete blocks in this area. Furthermore, the values of the Re index of the Am4 and C2 sub-basins (Table 2) indicate an anomalously elongated shape, suggesting, along with the high values of the S index (Table 2), a tectonic control with fast local uplift of the LCFS and SSPFS footwall blocks.

Table 2. Hierarchical parameters and geomorphic indexes of the three major river drainage networks.

Am4	**Number**	**Rb**	**Rbd**	**R = (Rb − Rbd)**	**An**	**AF**	**Re**	**S**
ord 1	742	5.7	3.7	1.9	255	58.40	0.184	1.62
ord 2	131	4.0	2.8	1.2	39			
ord 3	33	3.7	2.6	1.1	10			
ord 4	9	4.5	3.5	1.0	2			
ord 5	2	2.0	2.0	0.0	0			
ord 6	1							
C2	**Number**	**Rb**	**Rbd**	**R = (Rb − Rbd)**	**An**	**AF**	**Re**	**S**
ord 1	1117	5.6	3.6	2.0	395	25.82	0.171	1.58
ord 2	199	4.6	3.0	1.6	68			
ord 3	43	8.6	6.8	1.8	9			
ord 4	5	5.0	5.0	0.0	0			
ord 5	1							
A1	**Number**	**Rb**	**Rbd**	**R = (Rb − Rbd)**	**An**	**AF**	**Re**	**S**
ord 1	609	6.6	3.9	2.7	247	52.97	0.308	1.47
ord 2	92	5.4	3.9	1.5	26			
ord 3	17	4.3	3.0	1.3	5			
ord 4	4	2.0	2.0	0.0	0			
ord 5	2	2.0	2.0	0.0	0			
ord 6	1							

The computed hierarchical parameters of the Am4 and C2 sub-basins, such as the Rb, Rbd, R, and An values (Table 2), suggest a scant organization of the fluvial network, typical of recently rejuvenated drainage patterns. The hypsometric curve of these sub-basins shows a trend near to the youthful stage in the proximity of the SSPFS and the LCFS (Figures 7B and 8B), confirming such rejuvenation. Additionally, the shape of the longitudinal profiles of these two rivers shows an increase in the slope corresponding to the LCFS and a flat shape in the upper reach where the main river trunks flow parallel to the Fe and Fd belonging to the SSPFS (Figures 7C and 8C). Such evidence agrees with the prevalent normal motion of the LCFS and the strike-slip kinematics of the SSPFS.

Considering that the terrains on which the rivers flow do not show meaningful lithological change, the observed morphometric anomalies are considered of tectonic origin.

The recent activity of the SSPFS and the LCFS is also evidenced by a double fluvial capture of the fluvial network of the Am4 sub-basin at the expense of two old tributaries of the C2 sub-basin (Figure 9). The first capture occurred where the Fc crosses the Am4, and it is related to the uplift of the Fa and Fc footwalls that triggered a faster head retreat of the

young Am4 drainage, up to intercept the old sector of the C2 (Figure 9A,B). This piracy event is evidenced by wind gaps/suspended valleys, representing the abandoned drainage reaches of the C2 (see Figure 9C,D). The second capture event occurred in response to the progressive northward erosion of the Am4 fluvial network up to intercept the old C2 fluvial network. Such interception caused the Decollatura paleolake emptying (Figure 9E,F). Both the fluvial captures produced the clockwise deflection of the Am4 sub-basin (about 180 degrees).

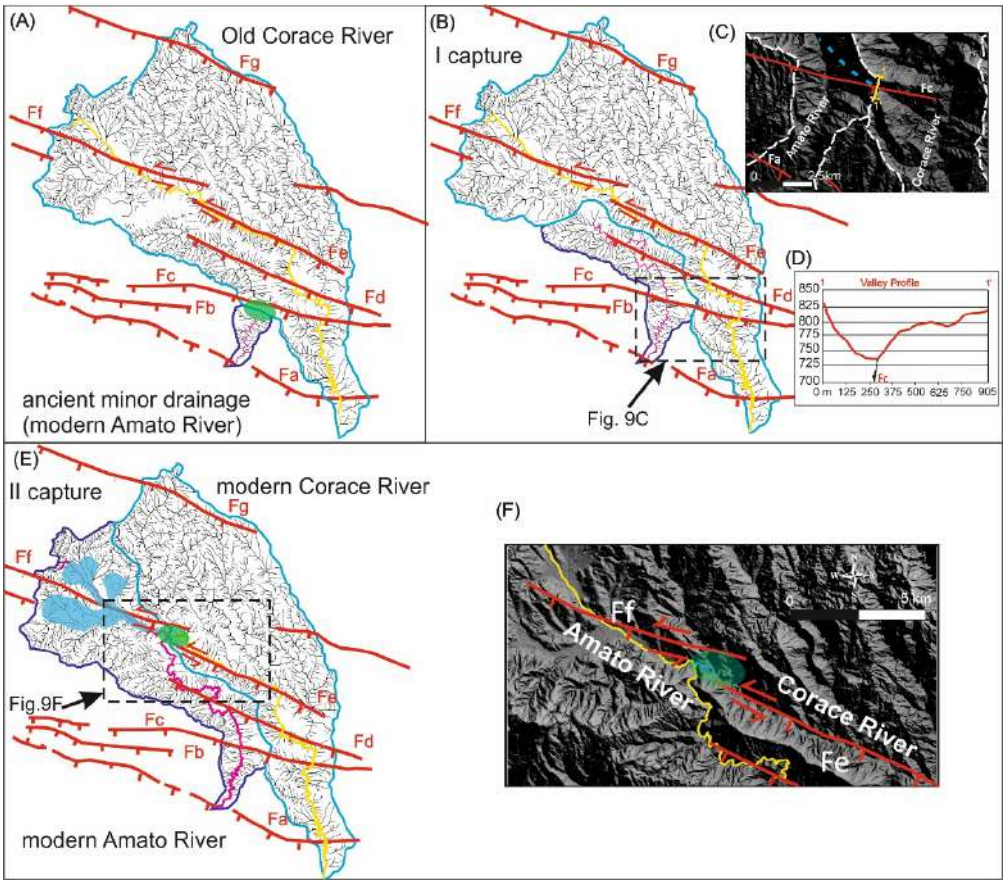

Figure 9. Reconstruction of the evolution of the fluvial network of Am4 sub-basin (blue polygon is the watershed, the pink line is the main river course) and fluvial network of C2 sub-basin (cyan polygon is the watershed, the yellow line is the main river course). (**A**) Ancient Am4 fluvial network (blue polygon), initially formed by minor drainage, and ancient C2 fluvial network (cyan polygon); the green ellipse indicates the zone of the fluvial catchment. (**B**) Fluvial network configuration after the first capture of the minor drainage (old Am4 fluvial network) at the expense of the old C2 fluvial network. (**C**) Detail of the fluvial capture of the old C2 fluvial network (see Figure 9B for location); blue dashed line is the track of the suspended valley. (**D**) Profile of the watershed (see the yellow trace 1-1′ in Figure 9C) showing the suspended valley and the track of Fc. (**E**) Second capture of the old C2 fluvial network and present-day configuration of the two rivers; green ellipse is the area of push-up and obstruction of the old C2 fluvial network; cyan polygon represents the Decollatura paleolake. (**F**) Detail of the northern capture; the cyan line inside the green ellipse is the old abandoned C2 drainage (see Figure 9E for location).

4.3. The Maida and Stalettì Faults

On the southern side of the Catanzaro Trough, the Maida and Stalettì faults show intensely eroded, low steep scarps, displacing upper Miocene–Pliocene deposits [12]. The Maida and Stalettì faults cross out the T1, Am5, and A1 sub-basins that are characterized by low to moderate values of Ksn, low slope, and low local relief values at the interception with these faults (Figure 6A–D). The A1 is the most developed sub-basin intercepted by

the Staletti Fault (Figure 10A). Outcomes from hierarchical parameters (i.e., T-factor, AF, Re, and S indexes) suggest that the Alessi River is relatively stable (Table 2). The stability of this river is evidenced by the mature stage of the hypsometric curve and by the eroded and mature profile of the main river trunk near the Staletti Fault (Figure 10B,C). Overall, geomorphological and morphometric data indicate weak or no recent activity of the Maida and Staletti faults.

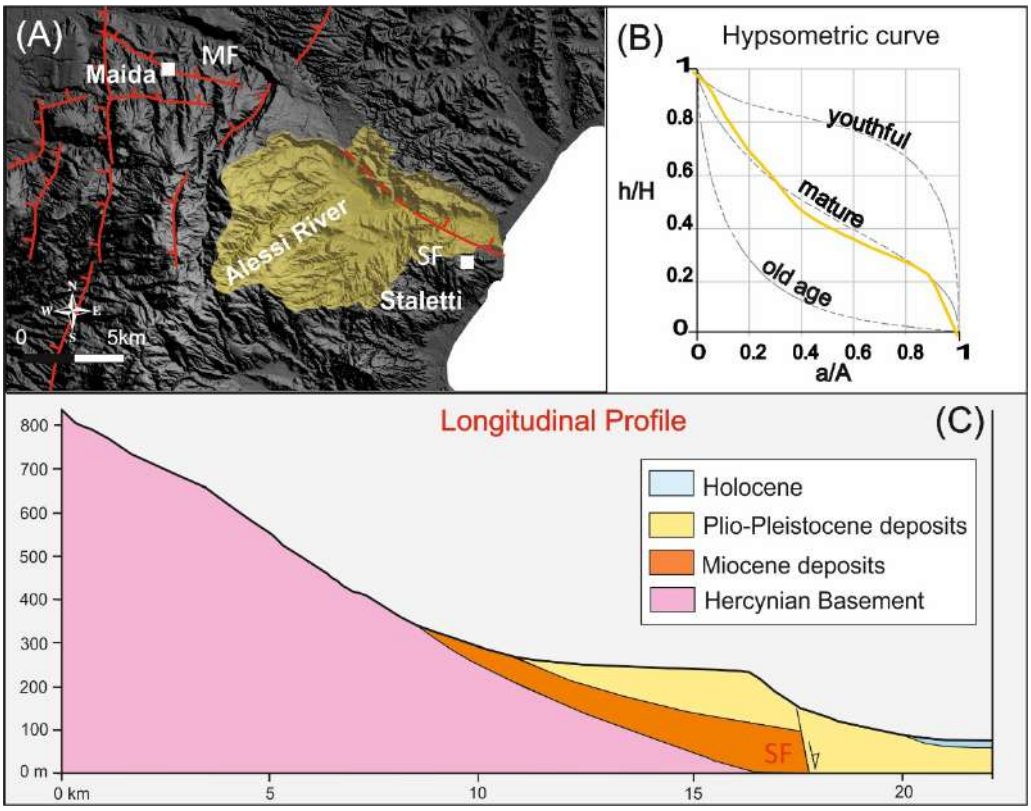

Figure 10. (**A**) DTM hillshade showing the Alessi sub-basin and faults crossing the area. (**B**) Hypsometric curve of the Alessi sub-basin. (**C**) Longitudinal profile of the main river trunk of the Alessi sub-basin.

4.4. The Caraffa Fault System

Although characterized by weak outcrop scale structural evidence, the Caraffa Fault System gives rise to geomorphological markers indicating its recent activity. The northernmost segments of the system (Cfa and Cfb) are responsible for differential block motion in the central sector of the Catanzaro Trough (Figure 2B). The Cfa segment is responsible for the tilting and warping of the III order marine terrace southwest of the Caraffa village (Figure 2F). The Cfb segment dislocates a morphological platform and causes the rejuvenation of the eastern side of a valley (Figure 2G). The morphological imprint of the Cfc segment is evident in profile B-B′ (Figure 4B), which shows a morphological scarp corresponding to the Cfc fault trace and the eastward tilting of the footwall. Furthermore, the western sector of the Catanzaro Trough, at the hanging wall of the Caraffa Fault System, is characterized by a well-preserved flat of marine terraces. Conversely, the eastern sector, especially at the footwall of the Cfc segment, is incised by deep V-shaped fluvial valleys.

The swath profile along the C-C′ track (Figure 4C) confirms the substantial variation in the relief distribution between the Tyrrhenian and the Ionian sectors of the Catanzaro Trough, passing from the hanging wall to the footwall of the Caraffa Fault System. In this profile, the lower standard deviation values, together with the more continuous topography of the western side, highlight a landscape currently related to the slow vertical motion that caused the formation of the staircase of marine terraces. On the contrary, the high standard

deviation values of the eastern side of the basin and the presence of numerous V-shaped valleys suggest the faster uplift of this sector.

The longitudinal profiles of the R1–R5 reaches of the Amato River show slope breaks and increases aligning with the Caraffa Fault System (Figure 5A–E), indicating that its persisting activity is not correlated to the values of the catchment area. The geometry of the R1–R5 reaches shows significative deflections (roughly 90 degrees) in the vicinity of the faults, which cause the river network to bend from a flow direction perpendicular to the fault towards a flow direction parallel to the fault (Figure 3B). Diffuse wind gaps, such as that observed between the Amato and Angitola Rivers (Figure 3C), suggest the persisting activity of the northernmost segment of the fault system.

Finally, T-factor values of the sub-basins located inside the Catanzaro Trough highlight that, in the nearness of the Caraffa Fault System, the main river trunks are anomalously shifted toward the east, against the track of the Cfa segment, suggesting the presence of a depocenter in the hanging wall of this fault (see T1-2 and Am3-5 in Figure 6E).

5. Seismotectonic Implications

The GNSS velocity field and its cross-section (Figures 11 and 12a) show that the Ionian sector of the Catanzaro Trough is characterized by velocities toward ESE greater than the Tyrrhenian side of the basin [9]. Such velocity difference highlights the ongoing extension process characterized by rates of about 1 mm/year, compatible with the activity of the NNE–SSW-trending extensional Caraffa Fault System.

The projection of the hypocentres of the instrumental earthquakes that occurred from 1985 to 2022 (from http://terremoti.ingv.it/, accessed on 15 July 2022, see also [54]) on a section roughly parallel to the Catanzaro Trough shows the Ionian plate dipping below the Tyrrhenian Sea (Figure 12b). Corresponding to the Caraffa Fault System, a sub-vertical alignment of hypocentres deepens to the limit of the seismogenic layer, suggesting the seismic activity of this structure (see also [9]). The 2019 seismic sequence (Mw up to 4) occurred west of the Caraffa village (Figure 1B); the focal mechanism of the main shock (Figure 11) and its projection at depth (Figure 12b) reveal the occurrence of a N–S-oriented normal fault plane that matches well with the geometry and kinematics of the Caraffa Fault System.

As regards to the large historical earthquakes that occurred in the Catanzaro Trough, several seismogenic sources have been modelled: the ITCS110 located in the western margin of the basin and related to the 1905 earthquake, which likely occurred in the Tyrrhenian offshore, and the ITCS068, which bounds the basin to the north and should be suitable to generate earthquakes with a magnitude up to 7.1 [15] (Figure 1B). The latter source partially coincides with the Lamezia–Catanzaro Fault System that, according to Pirrotta et al. [9], should be responsible for the historical and instrumental seismicity of the area, given the occurrence of earthquake clusters nucleated on these faults. Due to their location and geometry, these sources are not consistent with many of the earthquakes that occurred in the central and southern sectors of the Catanzaro Trough, such as those in 1626 A.D. and on 28 March 1783, respectively [14] (Figure 1B). Akinci et al. [13] modelled a NNE–SSW seismogenic source (ITES002) in the central sector of the basin (Figure 1B), based on geodynamic considerations. The seismic potential (roughly Mw 7 according to [13]) and its location and geometry make this source suitable for the large historical and instrumental seismicity of the Catanzaro Trough. Considering its location, geometry, and kinematics, the Caraffa Fault System matches the ITEES002 seismogenic source quite well. According to our morphometric analysis, this system is about 17 km long, even though it could have a length up to about 24 km at depth since the sub-surface rupture length (RLD) of a fault is generally longer than the rupture length at the surface (SRL) by up to 35–45% [64,65]. Thus, in our opinion, the Caraffa Fault System may generate earthquakes with a magnitude up to 6.7.

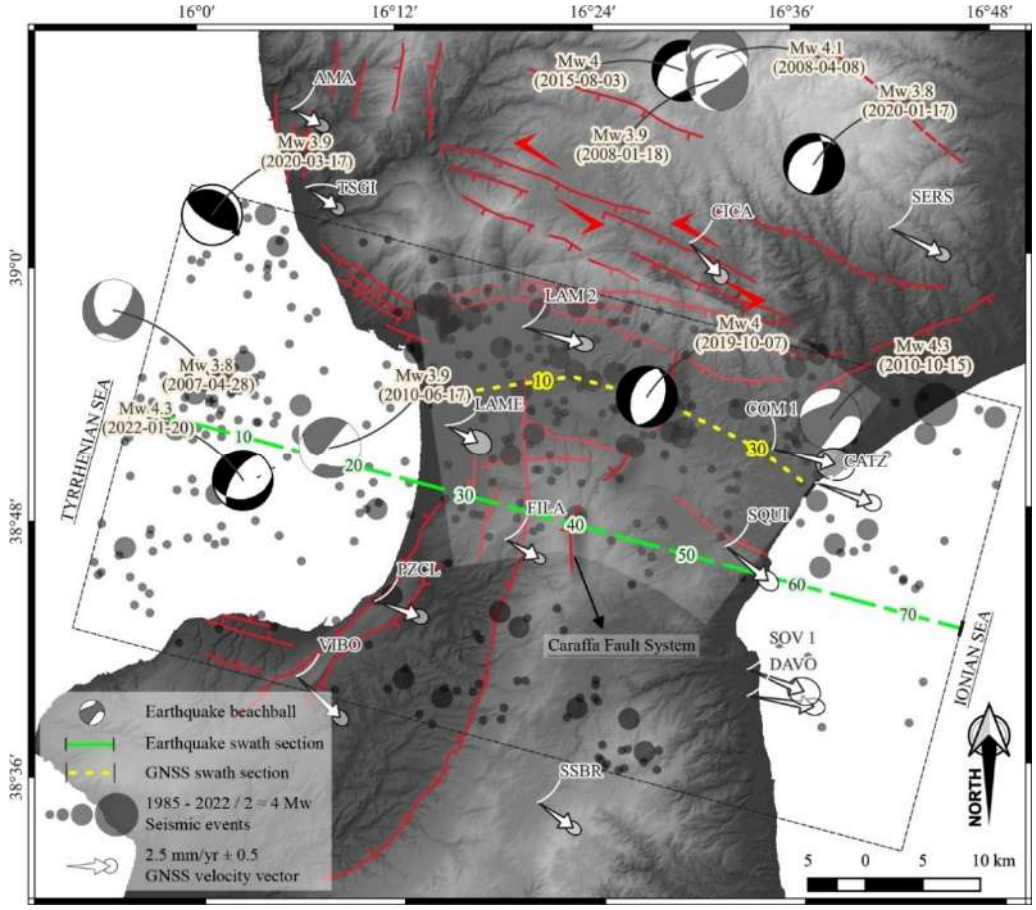

Figure 11. Seismotectonic map of the Catanzaro Trough. The beachballs and grey dots indicate the 1985–2022 instrumental and parametric seismicity (from http://terremoti.ingv.it/, accessed on 15 July 2022; see also [54]). White arrows represent the GNSS velocity field (from Pirrotta et al. [9]). The yellow dashed line and the whitish transparent polygon represent the swath baseline and area, respectively, of the GNSS velocity cross-section, plotted in Figure 12a. The green dashed line and the black dashed rectangle represent the swath baseline and area of the seismicity cross-section plotted in Figure 12b, respectively. The yellow and light green buffered numbers along the two dashed lines represent the distance along the lines expressed in km.

The seismic activity, highlighted by the alignment of the earthquakes at depth (Figure 12b), together with the parameterization (location, geometry, and kinematics), make the Caraffa Fault System a suitable candidate as a source responsible for the historical and instrumental seismicity of this sector of the Catanzaro Trough (including the 1626 A.D. and 28 March 1783 events and the seismic sequence of 2019; Figure 1B). According to Rovida et al. [14], the macroseismic epicentre of the 28 March 1783 event is located slightly to the southeast of the Caraffa Fault System, but the reconstruction of the macroseismic field could have been influenced by the localities already seriously damaged by the previous shocks of the 1783 seismic sequence, mainly located in southern Calabria [66]. Uncertainty about the epicentral location of this event may also be due to the deeper location of its hypocentre than the previous earthquakes of the 1783 seismic sequence, which makes the isoseismal gradient scantly steep and the felt area wider [66].

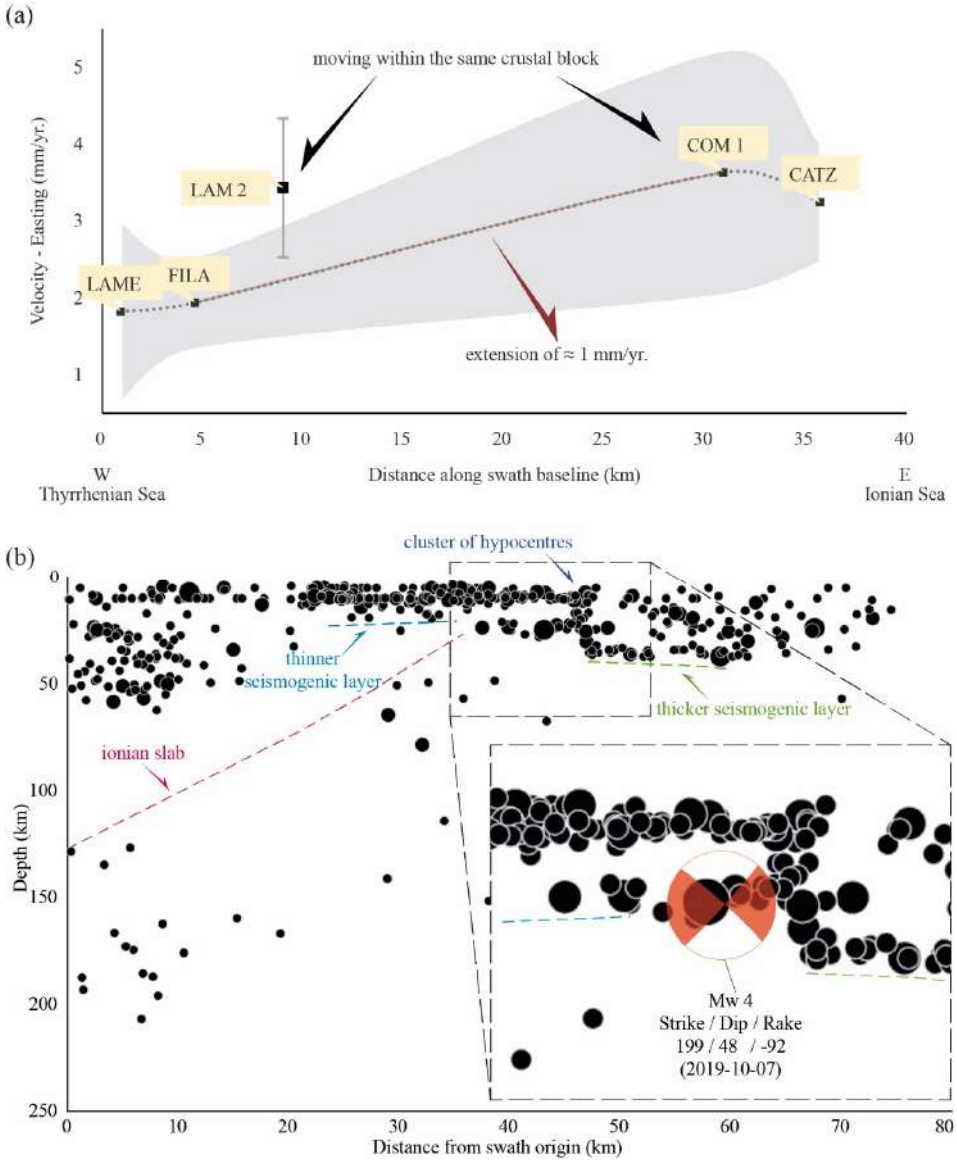

Figure 12. (**a**) GNSS velocity cross-section (data from Pirrotta et al. [9]) along the Catanzaro Trough showing a current extension in the Catanzaro Trough of about 1 mm/year (section trace is plotted in Figure 11). (**b**) Swath cross-section showing the earthquake hypocentre distribution (data from http://terremoti.ingv.it/, accessed on 15 July 2022, see also [54]) in the Catanzaro Trough (section trace is plotted in Figure 11). The beachball refers to the 2019 Mw 4 earthquake (see Figures 1 and 11 for location).

6. Conclusions

The geomorphological and morphometric study of the Catanzaro Trough and surrounding areas allowed us to improve the knowledge of the active tectonics of this crucial sector of the Calabrian Arc. The South Sila Piccola Fault System and the Lamezia–Catanzaro Fault System show the most significant evidence of Quaternary activity. The SSPS is characterized by left-lateral motion and accommodates the differential SE-ward advancement of the upper crustal level of the arc. The LCFS shows a prevalent normal component of motion and accommodates the transition from the strike-slip regime in the north to the extensional one in the south. Conversely, the normal faults bounding the Catanzaro Trough to the south (the MS and SF) do not show recent movement. Outcomes from the relief distribution and morphometric analyses made it possible to detect, for the first time, the geomorphological signature of the Caraffa Fault System, a NNE–SSW-trending, WSW-dipping extensional

structural alignment extending from the central portion of the Catanzaro Trough to the south. The Caraffa Fault System represents the northern prosecution of the Serre Fault, a major extensional structure that accommodates the WNW–ESE-oriented extension of the southern sector of the Calabrian Arc [9,66]. Given its location, geometry, and kinematics, and the instrumental seismicity recorded, the Caraffa Fault System may have been responsible for the strong historical earthquakes of this sector of the Calabrian Arc, such as the events of 1626 A.D. and 28 March 1783, and for this reason, it should be evaluated in the future definition of the seismic hazard of the area.

Author Contributions: C.P. and C.M.: Conceptualization, investigation, methodology, writing—original draft, writing—review and editing, data curation, supervision. N.P.: Investigation, methodology, writing—review and editing, data curation, visualization. F.P. and C.T.: Investigation, methodology, visualization. All authors have read and agreed to the published version of the manuscript.

Funding: This research was funded by the MUSE 4D project—Overtime tectonic, dynamic and rheologic control on destructive multiple seismic events—Special Italian Faults & Earthquakes: From real 4D cases to models in the frame of PRIN 2017 (grant number 2017KT2MKE).

Data Availability Statement: See text for links to publicly archived datasets analysed. Data supporting the reported results are available on request by email to the corresponding author (cmonaco@unict.it).

Acknowledgments: Two anonymous reviewers and the Editor are kindly acknowledged for their constructive comments and suggestions. The research was also performed in the frame of the Landscape Evolution Marker Online Network (LEMON) project (INQUA—AIQUA framework).

Conflicts of Interest: The authors declare no conflict of interest.

References

1. Ghisetti, F.; Vezzani, L. Different styles of deformation in the Calabrian arc (southern Italy): Implications for a seismotectonic zoning. *Tectonophysics* **1982**, *85*, 149–165. [CrossRef]
2. Monaco, C.; Tortorici, L.; Nicolich, R.; Cernobori, L.; Costa, M. From collisional to rifted basins: An example from the southern Calabrian arc (Italy). *Tectonophysics* **1996**, *266*, 233–249. [CrossRef]
3. Tortorici, L.; Monaco, C.; Tansi, C.; Cocina, O. Recent and active tectonics in the Calabrian arc (Southern Italy). *Tectonophysics* **1995**, *243*, 37–55. [CrossRef]
4. Monaco, C.; Tortorici, L. Active faulting in the Calabrian arc and eastern Sicily. *J. Geodyn.* **2000**, *29*, 407–424. [CrossRef]
5. Tansi, C.; Iovine, G.; Fòlino-Gallo, M. Tettonica attiva e recente, e manifestazioni gravitative profonde, lungo il bordo orientale del graben del Fiume Crati (Calabria settentrionale). *Boll. Soc. Geol. Ital.* **2005**, *124*, 563–578.
6. Tansi, C.; Muto, F.; Critelli, S.; Iovine, G. Neogene-Quaternary strike-slip tectonics in the central Calabria Arc (southern Italy). *J. Geodyn.* **2007**, *43*, 397–414. [CrossRef]
7. Van Dijk, J.P.; Bello, M.; Brancaleoni, G.P.; Cantarella, G.; Costa, V.; Frixa, A.; Golfetto, F.; Merlini, S.; Riva, M.; Torricelli, S.; et al. A regional structural model for the northern sector of the Calabrian Arc (southern Italy). *Tectonophysics* **2000**, *324*, 267–320. [CrossRef]
8. Brutto, F.; Muto, F.; Loreto, M.F.; De Paola, N.; Tripodi, V.; Critelli, S.; Facchin, L. The Neogene-Quaternary geodynamic evolution of the central Calabrian Arc: A case study from the western Catanzaro Trough basin. *J. Geodyn.* **2016**, *102*, 95–114. [CrossRef]
9. Pirrotta, C.; Barberi, G.; Barreca, G.; Brighenti, F.; Carnemolla, F.; De Guidi, G.; Monaco, C.; Pepe, F.; Scarfì, L. Recent Activity and Kinematics of the Bounding Faults of the Catanzaro Trough (Central Calabria, Italy): New Morphotectonic, Geodetic and Seismological Data. *Geosciences* **2021**, *11*, 405. [CrossRef]
10. Punzo, M.; Cianflone, G.; Cavuoto, G.; De Rosa, R.; Dominici, R.; Gallo, P.; Lirer, F.; Pelosi, N.; Di Fiore, V. Active and passive seismic methods to explore areas of active faulting. The case of Lamezia Terme (Calabria, southern Italy). *J. Appl. Geophys.* **2021**, *188*, 104316. [CrossRef]
11. Moretti, A. Il Database delle Faglie Capaci della Calabria: Stato Attuale delle Conoscenze. In *Progetto 5.1.2 Inventario delle Faglie Attive e dei Terremoti ad Esse Associabili*; Università della Calabria: Rende, Italy, 1999; Available online: https://emidius.mi.ingv.it/GNDT/P512/UR_UNICS.html (accessed on 15 July 2022).
12. Gullà, G.; Antronico, L.; Sorriso-Valvo, M.; Tansi, C. Proposta metodologica per la valutazione di indicatori di pericolo e rischio da frana a scala intermedia: L'area della Stretta di Catanzaro (Calabria, Italia). *Geol. Romana* **2005**, *38*, 97–112.
13. Akinci, A.; Vannoli, P.; Falcone, G.; Taroni, M.; Tiberti, M.M.; Murru, M.; Burrato, P.; Mariucci, M.T. When time and faults matter: Towards a time-dependent probabilistic SHA in Calabria, Italy. *Bull. Earthq. Eng.* **2017**, *15*, 2497–2524. [CrossRef]
14. Rovida, A.; Locati, M.; Camassi, R.; Lolli, B.; Gasperini, P.; Antonucci, A. *Italian Parametric Earthquake Catalogue (CPTI15), Version 3.0*; Istituto Nazionale di Geofisica e Vulcanologia (INGV): Roma, Italy, 2021. [CrossRef]

15. DISS Working Group. *Database of Individual Seismogenic Sources (DISS), Version 3.3.0: A Compilation of Potential Sources for Earthquakes Larger than M 5.5 in Italy and Surrounding Areas*; Istituto Nazionale di Geofisica e Vulcanologia (INGV): Roma, Italy, 2021.
16. Cox, R.T. Analysis of drainage basin symmetry as a rapid technique to identify areas of possible Quaternary tilt-block tectonics: An example from the Mississippi Embayment. *Geol. Soc. Am. Bull.* **1994**, *106*, 571–581. [CrossRef]
17. Burrato, P.; Ciucci, F.; Valensise, G. An inventory of river anomalies in the Po Plain, Northern Italy: Evidence for active blind thrust faulting. *Ann. Geophys.* **2003**, *46*, 865–882. [CrossRef]
18. Hare, P.W.; Gardner, T.W. Geomorphic indicators of vertical neotectonism along converging plate margins, Nicoya Peninsula, Costa Rica. In *Tectonic Geomorphology, Proceedings of the 15th Annual Binghamton Geomorphology Symposium, September 1984*; Morisawa, M., Pantosti, D., Eds.; Allen & Unwin: Boston, MA, USA, 1985; pp. 123–134.
19. Valensise, G.; Pantosti, D. The investigation of potential earthquake sources in peninsular Italy: A review. *J. Seismol.* **2001**, *5*, 287–306. [CrossRef]
20. Snyder, N.P.; Whipple, K.X.; Tucker, G.E.; Merritts, D.J. Landscape response to tectonic forcing: Digital elevation model analysis of stream profiles in the Mendocino triple junction region, northern California. *Geol. Soc. Am. Bull.* **2000**, *112*, 1250–1263. [CrossRef]
21. Whipple, K.X. Bedrock rivers and the geomorphology of active orogens. *Annu. Rev. Earth Planet. Sci.* **2004**, *32*, 151–185. [CrossRef]
22. Guarnieri, P.; Pirrotta, C. The response of drainage basins to the late Quaternary tectonics in the Sicilian side of the Messina Strait (NE Sicily). *Geomorphology* **2008**, *95*, 260–273. [CrossRef]
23. Pedrera, A.; Pérez-Peña, J.V.; Galindo-Zaldívar, J.; Azañón, J.M.; Azor, A. Testing the sensitivity of geomorphic indices in areas of low-rate active folding (eastern Betic Cordillera, Spain). *Geomorphology* **2009**, *105*, 218–231. [CrossRef]
24. Figueroa, A.M.; Knott, J.R. Tectonic geomorphology of the southern Sierra Nevada Mountains (California): Evidence for uplift and basin formation. *Geomorphology* **2010**, *123*, 34–45. [CrossRef]
25. Demoulin, A. Basin and river profile morphometry: A new index with a high potential for relative dating of tectonic uplift. *Geomorphology* **2011**, *126*, 97–107. [CrossRef]
26. Camafort, M.; Pérez-Peña, J.V.; Booth-Rea, G.; Melki, F.; Gràcia, E.; Azañón, J.M.; Galve, J.P.; Marzougui, W.; Gaidi, S.; Ranero, C.R. Active tectonics and drainage evolution in the Tunisian Atlas driven by interaction between crustal shortening and mantle dynamics. *Geomorphology* **2020**, *351*, 106954. [CrossRef]
27. Pirrotta, C.; Barbano, M.S. New Macroseismic and Morphotectonic Constraints to Infer a Fault Model for the 9 (Mw6.1) and 11 January (Mw7.3) 1693 Earthquakes (Southeastern Sicily). *Front. Earth Sci.* **2020**, *8*, 550851. [CrossRef]
28. Molin, P.; Pazzaglia, F.J.; Dramis, F. Geomorphic expression of the active tectonics in a rapidly-deforming forearc, Sila Massif, Calabria, Southern Italy. *Am. J. Sci.* **2004**, *304*, 559–589. [CrossRef]
29. Pirrotta, C.; Barbano, M.S.; Monaco, C. Evidence of active tectonics in Southern Calabria (Italy) by geomorphic analysis: The examples of the Catona and Petrace rivers. *Ital. J. of Geosci.* **2016**, *135*, 142–156. [CrossRef]
30. Roda-Boluda, D.C.; Whittaker, A.C. Structural and geomorphological constraints on active normal faulting and landscape evolution in Calabria, Italy. *J. Geol. Soc.* **2017**, *174*, 701–720. [CrossRef]
31. Carminati, E.; Wortel, M.J.R.; Spakman, W.; Sabadini, R. The role of slab detachment processes in the opening of the western–central Mediterranean basins: Some geological and geophysical evidence. *Earth Planet. Sci. Lett.* **1998**, *160*, 651–665. [CrossRef]
32. Faccenna, C. Constraints on mantle circulation around the deforming Calabrian slab. *Geophys. Res. Lett.* **2005**, *32*, L06311. [CrossRef]
33. Carminati, E.; Doglioni, C. Mediterranean tectonics. In *Encyclopedia of Geology*; Selley, R.C., Robin, L., Cocks, M., Plimer, I.R., Eds.; Elsevier Academic Press: Cambridge, MA, USA, 2005; pp. 135–146.
34. Guarnieri, P. Plio-Quaternary segmentation of the south Tyrrhenian forearc basin. *Int. J. Earth Sci. (Geol. Rundsch.)* **2006**, *95*, 107–118. [CrossRef]
35. Pepe, F.; Bertotti, G.; Ferranti, L.; Sacchi, M.; Collura, A.M.; Passaro, S.; Sulli, A. Pattern and rate of post-20 ka vertical tectonic motion around the Capo Vaticano Promontory (W Calabria, Italy) based on offshore geomorphological indicators. *Quat. Int.* **2014**, *332*, 85–98. [CrossRef]
36. Tiberti, M.M.; Vannoli, P.; Fracassi, U.; Burrato, P.; Kastelic, V.; Valensise, G. Understanding seismogenic processes in the Southern Calabrian Arc: A geodynamic perspective. *Ital. J. Geosci.* **2017**, *136*, 365–388. [CrossRef]
37. De Ritis, R.; Pepe, F.; Orecchio, B.; Casalbore, D.; Bosman, A.; Chiappini, M.; Chiocci, F.; Corradino, M.; Nicolich, R.; Martorelli, E.; et al. Magmatism along lateral slab-edges: Insights from the Diamante-Enotrio-Ovidio Volcanic-Intrusive Complex (Southern Tyrrhenian Sea). *Tectonics* **2019**, *38*, 2581–2605. [CrossRef]
38. Corradino, M.; Pepe, F.; Bertotti, G.; Picotti, V.; Monaco, C.; Nicolich, R.; et al. 3-D Architecture and Plio-Quaternary Evolution of the Paola Basin: Insights into the Forearc of the Tyrrhenian-Ionian Subduction System. *Tectonics* **2020**, *39*, e2019TC005898. [CrossRef]
39. Corradino, M.; Pepe, F.; Burrato, P.; Kanari, M.; Parrino, N.; Bertotti, G.; Bosman, A.; Casalbore, D.; Ferranti, L.; Martorelli, E. An integrated multiscale method for the characterisation of active faults in offshore areas. The case of Sant'Eufemia Gulf (Offshore Calabria, Italy). *Front. Earth Sci.* **2021**, *9*, 670557. [CrossRef]
40. Wortel, R.; Spakman, W. Subduction and slab detachment in the Mediterranean-Carpathian region. *Science* **2000**, *290*, 1910–1917. [CrossRef]
41. Orecchio, B.; Presti, D.; Totaro, C.; Neri, G. What earthquakes say concerning residual subduction and STEP dynamics in the Calabrian Arc region, south Italy. *Geophys. J. Intern.* **2014**, *199*, 1929–1942. [CrossRef]

42. Maesano, F.E.; Tiberti, M.M.; Basili, R. The Calabrian Arc: Three-dimensional modelling of the subduction interface. *Sci. Rep.* **2017**, *7*, 8887. [CrossRef]
43. Scarfì, L.; Barberi, G.; Barreca, G.; Cannavò, F.; Koulakov, I.; Patanè, D. Slab narrowing in the Central Mediterranean: The Calabro-Ionian subduction zone as imaged by high resolution seismic tomography. *Sci. Rep.* **2018**, *8*, 5178. [CrossRef]
44. Barreca, G.; Scarfì, L.; Gross, F.; Monaco, C.; De Guidi, G. Fault pattern and seismotectonic potential at the south-western edge of the Ionian Subduction system (southern Italy): New field and geophysical constraints. *Tectonophysics* **2019**, *761*, 31–45. [CrossRef]
45. Westaway, R. Quaternary uplift of southern Italy. *J. Geophys. Res.* **1993**, *98*, 741–772. [CrossRef]
46. Doglioni, C.; Innocenti, F.; Mariotti, G. Why Mt. Etna? *Terra Nova* **2001**, *13*, 25–31. [CrossRef]
47. Miyauchi, T.; Dai Pra, G.; Labini, S.S. Geochronology of Pleistocene marine terraces and regional tectonics in the Tyrrhenian coast of south Calabria, Italy. *Il Quat.* **1994**, *7*, 17–34.
48. Monaco, C.; Barreca, G.; Di Stefano, A. Quaternary marine terraces and fault activity in the northern mainland sectors of the Messina Straits (southern Italy). *Ital. J. Geosci.* **2017**, *136*, 337–346. [CrossRef]
49. Amodio Morelli, L.; Bonardi, G.; Colonna, V.; Dietrich, D.; Giunta, G.; Ippolito, F.; Liguori, V.; Lorenzoni, S.; Paglionico, A.; Perrone, V.; et al. L'Arco Calabro-Peloritano nell'orogene Appenninico-Maghrebide. *Mem. Della Soc. Geol. Ital.* **1976**, *17*, 1–60.
50. Zecchin, M.; Praeg, D.; Ceramicola, S.; Muto, F. Onshore to offshore correlation of regional unconformities in the Plio-Pleistocene sedimentary successions of the Calabrian Arc (central Mediterranean). *Earth Sci. Rev.* **2015**, *142*, 60–78. [CrossRef]
51. Ouchi, S. Response of alluvial rivers to slow active tectonic movement. *Geol. Soc. Am. Bull.* **1985**, *96*, 504–515. [CrossRef]
52. Parrino, N.; Pepe, F.; Burrato, P.; Dardanelli, G.; Corradino, M.; Pipitone, C.; Gasparo Morticelli, M.; Sulli, A.; Di Maggio, C. Elusive active faults in a low strain rate region (Sicily, Italy): Hints from a multidisciplinary land-to-sea approach. *Tectonophysics* **2022**, *839*, 229520. [CrossRef]
53. O'Callaghan, J.F.; Mark, D.M. The extraction of drainage networks from digital elevation data. *Comput. Vis. Graph. Image Process.* **1984**, *28*, 323–344. [CrossRef]
54. ISIDe Working Group. Italian Seismological Instrumental and Parametric Database (ISIDe). Istituto Nazionale di Geofisica e Vulcanologia (INGV): Roma, Italy, 2007. [CrossRef]
55. Horton, R. E. Erosional development of streams and their drainage basins. Hydro-physical approach to quantitative morphology. *Geol. Soc. of Am. Bull.* **1945**, *56*, 275–370. [CrossRef]
56. Strahler, A.N. Hypsometric (area-altitude) analysis of erosional topography. *Geol. Soc. Am. Bull.* **1952**, *63*, 1117–1142. [CrossRef]
57. Avena, G.C.; Giuliano, G.; Lupia Palmieri, E. Sulla valutazione quantitativa della gerarchizzazione ed evoluzione dei reticoli fluviali. *Boll. Soc. Geol. Ital.* **1967**, *86*, 781–796.
58. Pinter, N. Applications of tectonic geomorphology for deciphering active deformation in the Pannonian Basin Hungary. In *Proceedings of the Workshop on Applications of GPS in Plate Tectonics in Research on Fossil Energy Resources and in Earthquake Hazard Assessment*; Fodor, L., Brezsnyánszky, K., Eds.; Occasional Papers of the Geological Institute of Hungary; Magyar Állami Földtani Intézet: Budapest, Hungary, 2005; Volume 204, pp. 25–51.
59. Bull, W.B.; McFadden, L. Tectonic geomorphology north and south of the Garlock Fault, California. In *Geomorphology in Arid Regions*; Doering, D.O., Ed.; State University of New York: Binghamton, NY, USA, 1977; pp. 115–138.
60. Woolderink, H.A.G.; Cohen, K.M.; Kasse, C.; Kleinhans, M.G.; Van Balen, R.T. Patterns in river channel sinuosity of the Meuse, Roer and Rhine rivers in the Lower Rhine Embayment rift-system, are they tectonically forced? *Geomorphology* **2021**, *375*, 107550. [CrossRef]
61. Kirby, E.; Whipple, K.X. Expression of active tectonics in erosional landscapes. *J. Struct. Geol.* **2012**, *44*, 54–75. [CrossRef]
62. Wobus, C.; Whipple, K.X.; Kirby, E.; Snyder, N.; Johnson, J.; Spyropolou, K.; Crosby, B.; Sheehan, D. Tectonics from topography: Procedurses, promise, and pitfalls. *Geol. Soc. Am. Spec. Pap.* **2006**, *398*, 55–74. [CrossRef]
63. Cassa per il Mezzogiorno. *Carta Geologica della Calabria. Tav. Decollatura*; Scale 1:25,000; Poligrafica & Cartevalori: Napoli, Italy, 1969.
64. Wells, D.; Coppersmith, K. New empirical relationships among magnitude, rupture length, rupture width, rupture area, and surface displacement. *Bull. Seismol. Soc. Am.* **1994**, *84*, 974–1002.
65. Boncio, P.; Lavecchia, G.; Pace, B. Defining a model of 3D seismogenic sources for seismic hazard assessment applications: The case of central Apennines (Italy). *J. Seismol.* **2004**, *8*, 407–425. [CrossRef]
66. Jacques, E.; Monaco, C.; Tapponnier, P.; Tortorici, L.; Winter, T. Faulting and earthquake triggering during the 1783 Calabria seismic sequence. *Geophys. J. Int.* **2001**, *147*, 499–516. [CrossRef]